International Journal of Solids and Structures 46 (2009) 3209–3221

Contents lists available at ScienceDirect

International Journal of Solids and Structures

journal homepage: www.elsevier.com/locate/ijsolstr

Underwater blast loading of sandwich beams: Regimes of behaviour

M.T. Tilbrook [1], V.S. Deshpande *, N.A. Fleck

Department of Engineering, University of Cambridge, Trumpington Street, Cambridge CB2 1PZ, UK

ARTICLE INFO

Article history:
Received 12 September 2007
Received in revised form 28 January 2009
Available online 23 April 2009

Keywords:
Lattice cores
Fluid–structure interaction
Sandwich panel
Finite element method

ABSTRACT

Finite element (FE) calculations are used to develop a comprehensive understanding of the dynamic response of sandwich beams subjected to underwater blast loading, including the effects of fluid–structure interaction. Design maps are constructed to show the regimes of behaviour over a broad range of loading intensity, sandwich panel geometry and material strength. Over the entire range of parameters investigated, the time-scale associated with the initial fluid–structure interaction phase up to the instant of first cavitation in the fluid is much smaller than the time-scales associated with the core compression and the bending/stretching responses of the sandwich beam. Consequently, this initial fluid–structure interaction phase decouples from the subsequent phases of response. Four regimes of behaviour exist: the period of sandwich core compression either couples or decouples with the period of the beam bending, and the core either densifies partially or fully. These regimes of behaviour are charted on maps using axes of blast impulse and core strength. The simulations indicate that continued loading by the fluid during the core compression phase and the beam bending/stretching phase cannot be neglected. Consequently, analyses that neglect full fluid–structure interaction during the structural responses provide only estimates of performance metrics such as back face deflection and reaction forces at the supports. The calculations here also indicate that appropriately designed sandwich beams undergo significantly smaller back face deflections and exert smaller support forces than monolithic beams of equal mass. The optimum transverse core strength is determined for minimizing the back face deflection or support reactions at a given blast impulse. Typically, the transverse core strength that minimizes back face deflection is 40% below the value that minimizes the support reaction. Moreover, the optimal core strength depends upon the level of blast impulse, with higher strength cores required for higher intensity blasts.

1. Introduction

A major consideration in the design of marine military vehicles is their resistance to underwater blast loading. Early work (at the time of World War II) focused on monolithic plates, and involved the measurement of blast resistance by full scale testing for a limited range of materials and geometries.

The main characteristics of a shock wave resulting from an underwater explosion are well established due to a combination of detailed large-scale experiments and modelling over the past 60 years. Useful summaries of the main phenomena are provided by Cole (1948) and Swisdak (1978) and are repeated briefly here in order to underpin the current study. The underwater detonation of a high explosive charge converts the solid explosive material into gaseous reaction products on a time scale of microseconds. The reaction products are at an enormous pressure: on the order of GPa, and this pressure is transmitted to the surrounding water by the propagation of a spherical shock wave at approximately sonic speed. Consider the response of a representative fluid element at a radial distance r from the explosion. Upon arrival of the primary shock wave, the pressure rises to a peak value p_0 almost instantaneously. Subsequently, the pressure decreases at a nearly exponential rate, with a time constant θ on the order of milliseconds. The magnitude of the shock wave peak pressure and decay constant depend upon the mass and type of explosive material and the distance r. After the primary shock wave has passed, subsequent secondary shocks are experienced, due to the damped oscillation of the gas bubble which contains the explosive reaction products. However, these secondary shock waves have much smaller peak pressures, and are usually much less damaging than the primary shock to a structure in the vicinity of the explosion than the primary shock.

A detailed overview on the shock response of monolithic beams and plates has been given by Jones (1989). More particularly Wang and Hopkins (1954) and Symmonds (1954) have analyzed the impulsive response of clamped circular plates and beams. However, their analyses were restricted to small deflections and linear bending kinematics. By direct application of the principle of virtual work for an assumed deformation mode, Jones (1971) presented an

* Corresponding author. Tel.: +44 1223 332664; fax: +44 1223 332662.
E-mail addresses: mttilbrook@gmail.com (M.T. Tilbrook), vsd@eng.cam.ac.uk (V.S. Deshpande).
[1] Present address: Moor Park Capital Partners, London, UK.

0020-7683/$ - see front matter © 2009 Elsevier Ltd. All rights reserved.
doi:10.1016/j.ijsolstr.2009.04.012

approximate solution for simply supported circular monolithic plates undergoing finite deflections. Experiments on impulsively loaded beams and plates have confirmed the deformation modes predicted by these analyses and also revealed a range of failure modes (Menkes and Opat, 1973; Nurick and Shave, 2000). Theoretical studies by Lee and Wierzbicki (2005a,b) have analyzed the so-called discing and petalling failure modes in impulsively loaded clamped plates while Balden and Nurick (2005) have analysed the so-called shear rupture modes. More recent efforts have focussed on the underwater blast response of sandwich beams and plates. The prototypical problem is sketched in Fig. 1, where a planar underwater blast wave impinges the entire sandwich beam. In this study we present a comprehensive numerical investigation of the deformation mechanisms and regimes for sandwich beams subjected to an underwater blast with an emphasis on the significance of the fluid–structure interaction (FSI) effect.

Over the past decade there have been substantial changes in ship design, see for example the review by Paik (2003). The main innovation has been the use of sandwich construction, with a range of topologies for the sandwich core. Several recent studies have shown that sandwich structures subjected to underwater blast loading outperform monolithic structures of equal mass, see for example Fleck and Deshpande (2004) and Xue and Hutchinson (2004). However, the relation between the sandwich core material properties and the sandwich beam performance remains unclear. Fleck and Deshpande (2004) have developed an analytical model for the shock resistance of clamped sandwich beams by separating the response of these beams into three sequential stages: the fluid–structure interaction stage I up to the point of first cavitation of the fluid, the core compression stage II and finally a combined beam bending and stretching stage III. The model of Fleck and Deshpande (2004) temporally decouples the three stages of the sandwich beam responses and provides a framework for understanding the blast response of sandwich beams. Recent finite element (FE) simulations by Rabczuk et al. (2004), Liang et al. (2007) and McShane et al. (2007) suggest that the Fleck and Deshpande (2004) model may over-estimate or under-estimate the deflection of a sandwich beam under blast loading due to cross-coupling between the three stages of the response. For example, the FE calculations of Rabczuk et al. (2004) suggest that cross-coupling between the initial fluid–structure interaction stage and the subsequent core compression stage increases the impulse transmitted into the sandwich beam and thereby leads to larger deflections. In contrast, for the so-called "soft cores" as analysed by Liang et al. (2007) and McShane et al. (2007), coupling between core compression in Stage II and combined beam bending and stretching of Stage III results in smaller back face deflections than predicted by the decoupled Fleck and Deshpande (2004) analysis.

Liang et al. (2007) suggest that a "soft core" minimizes both the back face deflections of the sandwich beams and the forces transmitted to the supporting structure. However, soft-core panels suffer from the drawback that they undergo face-sheet slap for high values of the blast impulse. Face-sheet slap significantly degrades their performance, as discussed by Hanssen et al. (2002), Nesterenko (2003), Yen et al. (2005) and Tilbrook et al. (2006).

Only limited experimental data exist on the underwater blast performance of clamped sandwich beams or plates due to the difficulty and expense of large-scale tests. Recently, Wei et al. (2007) have used a paddle-wheel apparatus to compare the blast responses of sandwich and monolithic plates when subjected to an identical water blast. They find that the back face deflections of

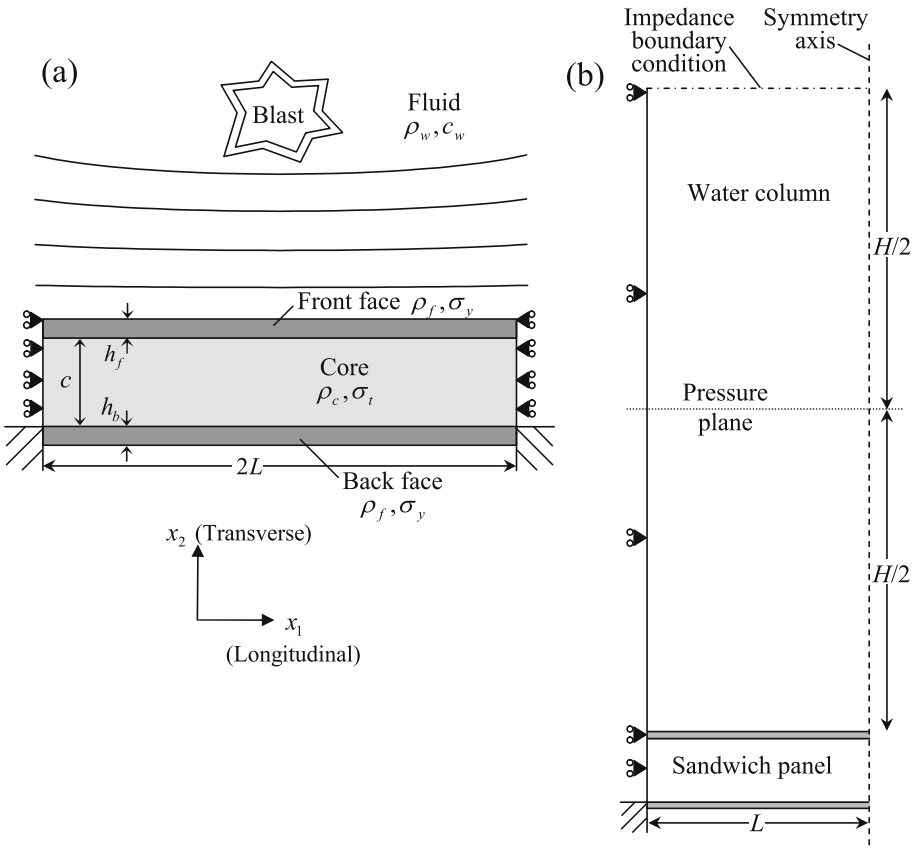

Fig. 1. (a) Geometry of the sandwich beam and schematic of the problem under consideration. (b) Sketch illustrating key boundary conditions employed in the fully-coupled fluid–structure interaction FE calculations.

sandwich beams with a honeycomb core are approximately equal to those of monolithic plates of equal mass.

In summary, conflicting views exist in the literature on the optimal designs and deformation mechanisms of sandwich beams subjected to an underwater blast. This is primarily due to the fact that most studies have considered a narrow range of blast impulses and sandwich beam properties, and the response is sensitive to these assumed values. In the current study, we present a comprehensive investigation that clarifies the various deformation mechanisms in terms of design maps with axes of sandwich core properties and blast impulse. The significance of FSI during the various stages of the deformation of the sandwich beams is also elucidated in order to gauge the validity of the various decoupled analyses.

2. Overview of the dynamic response of sandwich beams

Consider a sandwich beam of span $2L$, core thickness c and identical front and back face-sheets of thickness h as sketched in Fig. 1a. The core of density ρ_c is made from a rigid-ideally plastic compressible solid of uniaxial yield strengths σ_t and σ_l in the through-thickness transverse and longitudinal directions, respectively. (The tensile and compressive yield values are taken to be equal.) It is assumed that the plastic component of compressive strain within the foam-like core cannot exceed the nominal compressive densification strain ε_D. The face-sheet material has a density ρ_f and is rigid-ideally plastic with a tensile strength σ_Y. As outlined in the introduction, Fleck and Deshpande (2004) split the blast response of the sandwich structure into three sequential stages: *Stage I* is the fluid–structure interaction phase; *Stage II* is the core compression phase, and *Stage III* is the beam bending and stretching phase. The coupling between these three stages is now reviewed in order to aid interpretation of the finite element simulations reported below.

2.1. Coupling of stages I and II

Taylor (1963) developed the solution for a one-dimensional wave impinging a free-standing plate including the momentum transmitted to the plate by the shock pulse. Fleck and Deshpande (2004) made use of the Taylor calculation in order to estimate the momentum transmitted to a sandwich beam: they treated the front (wet) face of the sandwich beam as a free-standing plate.

Consider a planar pressure wave travelling at a velocity c_w in a fluid of density ρ_w. The wave passes any arbitrary point at time $t = 0$ and exerts on the fluid element the pressure transient

$$p = p_0 e^{-t/\theta} \tag{1}$$

where p_0 is the peak pressure and θ the decay constant of the wave. When this pressure wave impinges a *stationary* rigid plate at normal incidence it imparts an impulse of magnitude

$$I_0 \equiv 2\int_0^\infty p_0 e^{-t/\theta}\, dt = 2p_0\theta \tag{2}$$

to the plate. The factor of two arises in relation (2) due to full reflection of the pressure wave. If instead, the pressure wave impacts a free-standing plate, the imparted impulse is less than I_0, and can be estimated as follows. When the pressure wave strikes a free-standing plate of thickness h made from a material of density ρ_f it sets the plate in motion and is partially reflected. The precise response is dictated by the value of the Taylor fluid–structure interaction parameter, $\psi \equiv \rho_w c_w \theta/(\rho_f h)$. For example, the plate achieves its maximum velocity after a time

$$t_{cav} = \frac{\theta}{\psi - 1}\ln\psi. \tag{3}$$

At this instant the pressure at the interface between the plate and the fluid is zero and cavitation sets in. The momentum per unit area I_T transmitted to the structure is given by

$$I_T \equiv \psi^{\psi/(1-\psi)} I_0. \tag{4}$$

Fleck and Deshpande (2004) assumed that this transmitted impulse imparts a uniform velocity $v_0 = I_T/(\rho_f h)$ to the front (wet) face of the sandwich plate: recall that their analysis neglects the presence of the core and back (dry) face-sheet. Alternatively, an upper bound on the transmitted momentum can be obtained by considering the mass of the entire sandwich beam in the Taylor analysis rather than just the mass of the front face. The transmitted momentum is then given by

$$I_T \equiv \psi_f^{\psi_f/(1-\psi_f)} I_0, \tag{5}$$

in terms of the modified Taylor parameter $\psi_f \equiv \rho_w c_w \theta/(2\rho_f h + \rho_c c)$.

Several modifications to the Taylor model have been developed in order to include the effect of the crushing resistance of the core upon the momentum transmitted to the sandwich structure (Hutchinson and Xue, 2005; Deshpande and Fleck, 2005). These estimates lie between the two bounds given by Eqs. (4) and (5) and suggest that, for most practical designs, Eq. (4) underestimates the momentum transmitted into a sandwich plate by 20–40%. The additional momentum accounts for the discrepancies between the FE simulations of Rabczuk et al. (2004) and the analytical predictions of Fleck and Deshpande (2004).

2.2. Coupling of stages II and III

Tilbrook et al. (2006) have developed an analytical model for *impulsively-loaded* clamped sandwich beams that accounts for the coupling between the core compression and beam bending/stretching stages. They analyzed the independent motion of the front and back faces using a lumped mass approximation, such that the mass of the core is distributed equally and uniformly over the front and back face-sheets. The front face is decelerated by the crushing resistance of the core while the back face is a clamped monolithic beam, loaded by the core crushing strength σ_t. Their analysis revealed two characteristic time-scales: (i) the time t_{eq} at which the velocities of the front and back faces equalize and (ii) the time t_{bd} at which the back face starts to decelerate due to the reaction forces exerted by the supports dominating the force from the core. They identified four regimes of behaviour of the sandwich beam, depending upon the magnitudes of t_{eq} and t_{bd} in relation to the time t_D for core densification

Regime A: decoupled core compression and beam bending phases with partial core densification.
Regime B: decoupled core compression and beam bending phases with full core densification.
Regime C: coupled core compression and beam bending phases with partial core densification.
Regime D: coupled core compression and beam bending phases with full core densification.

Schematics of the typical temporal variations of the mid-span front face velocity v_f and back face velocity v_b for each of these four regimes are sketched in Fig. 2. Tilbrook et al. (2006) developed maps to summarise the dynamic response as a function of core strength, blast impulse and sandwich beam aspect ratio. The cross-coupling within regimes C and D leads to a reduced rear face deflection compared with the predictions of previous decoupled analyses such as Fleck and Deshpande (2004). However, the so-called "soft-core" regimes C and D occur over a relatively narrow range of core strength and sandwich beam geometry, specifically

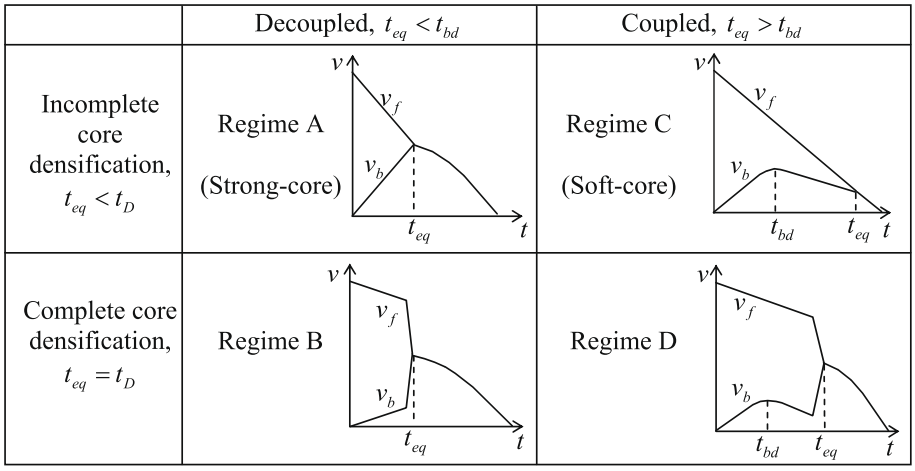

Fig. 2. The time history of front back face velocity for the four regimes of response. From Tilbrook et al. (2006).

a high value of c/L and a core of low transverse strength. We now investigate the fully-coupled fluid–structure interaction response of sandwich beams subjected to an underwater blast.

3. Finite element simulations

All computations were performed using the explicit time integration version of the commercially available FE code ABAQUS (version 6.5). The beams were modelled using four noded plane quadrilateral elements with reduced integration (type CPE4R in ABAQUS notation). Numerical damping associated with volumetric straining in ABAQUS Explicit was switched off; preliminary calculations revealed that the default viscosity in ABAQUS results in substantial and misleading artificial viscous dissipation during the large volumetric compression of the core. In all calculations reported in this section, the sandwich beams have face-sheets of thicknesses $h = 0.01$ m and a core of depth $c = 0.1$ m, giving $\bar{h} \equiv h/c = 0.1$. Finite element simulations were performed for selected values of sandwich aspect ratio $\bar{c} \equiv c/L$, as obtained by varying the half-span of the beam over the range $0.2\text{ m} \leqslant L \leqslant 1\text{ m}$. A uniform mesh with square elements of size $c/50$ was employed for core and face sheet in all calculations. Mesh sensitivity studies revealed that additional mesh refinements did not improve the accuracy of the calculations appreciably.

The blast resistance of monolithic beams was also determined for comparison purposes. These beams, of height H_m, were modelled by four-noded plane quadrilateral elements of side $H_m/10$; reduced integration was employed (CPE4R in the ABAQUS notation).

3.1. Constitutive models

The face-sheets of the sandwich beams and the monolithic beams are treated as an isotropic elastic-ideally plastic solid of Youngs' modulus E_f, Poisson ratio ν_f and uniaxial yield strength σ_Y. The solid yields in accordance with J2 flow theory, with a yield strain $\varepsilon_Y \equiv \sigma_Y/E_f$ and a density ρ_f.

The sandwich core is an orthotropic, compressible viscoplastic continuum, as specified previously by Tilbrook et al. (2006). This model is not meant to represent a particular cellular core but rather a generic compressive material whose properties can be readily modified to perform the parametric study presented in Section 4. The orthotropic axes x_i of the core are aligned with the axes of the beam as sketched in Fig. 1, i.e. x_1 and x_2 are aligned with the longitudinal and transverse directions, respectively. Making use of this co-ordinate frame, introduce the stress and plastic strain vectors in the usual way as

$$\boldsymbol{\sigma} = (\sigma_1, \sigma_2, \sigma_3, \sigma_4, \sigma_5, \sigma_6)^T \equiv (\sigma_{11}, \sigma_{22}, \sigma_{33}, \sigma_{13}, \sigma_{23}, \sigma_{12})^T, \tag{6}$$

and

$$\boldsymbol{\varepsilon}^p = \left(\varepsilon_1^p, \varepsilon_2^p, \varepsilon_3^p, \varepsilon_4^p, \varepsilon_5^p, \varepsilon_6^p\right)^T \equiv \left(\varepsilon_{11}^p, \varepsilon_{22}^p, \varepsilon_{33}^p, \varepsilon_{13}^p, \varepsilon_{23}^p, \varepsilon_{12}^p\right)^T, \tag{7}$$

respectively. Assume complete decoupling of material response between the orthogonal material directions. In order to capture shock formation under dynamic loading we model the foam as a rate sensitive material with the plastic strain rate $\dot{\varepsilon}_i^p$ obtained via the overstress relation

$$\dot{\varepsilon}_i^p = \begin{cases} \left(\frac{|\sigma_i| - Y_i(\varepsilon_i^p)}{\eta}\right) & \text{if } |\sigma_i| > Y_i(\varepsilon_i^p) \\ 0 & \text{otherwise,} \end{cases} \tag{8}$$

where the yield strength $Y_i(\varepsilon_i^p)$ is a function only of the plastic strain ε_i^p, with no cross-hardening. The material viscosity η is taken to be a constant-this viscosity is a numerical parameter used to numerically capture the shock rather than a "real" material rate sensitivity. The total strain rate $\dot{\varepsilon}_i$ is obtained by supplementing the above anisotropic plasticity model with isotropic elasticity such that

$$\dot{\varepsilon}_i = L_{ij}\dot{\sigma}_j + \dot{\varepsilon}_i^p \text{sign}(\sigma_i) \quad \text{(summation over } j\text{)}. \tag{9}$$

Here, the isotropic compliance matrix L_{ij} is specified in terms of the Young's modulus E_c and Poisson's ratio ν_c. This approach is justified by the observation that the core is subjected to large plastic strains and so it is important to represent it by an anisotropic yield surface, while isotropic elasticity is adequate for our purposes. The constitutive law for the core has been implemented in ABAQUS Explicit via the user-defined material subroutine VUMAT.

Material properties of the sandwich beam used in the numerical simulations are taken to be as follows. The face-sheets are made from an alloy of yield strength $\sigma_Y = 200$ MPa, yield strain $\varepsilon_Y = 0.1\%$, elastic Poisson's ratio $\nu_f = 0.3$ and density $\rho_f = 8000\text{ kg m}^{-3}$. The core is made from the same material and has a relative density $\bar{\rho} = 0.02$ (i.e. a core density $\rho_c = 160\text{ kg m}^{-3}$). The core is ascribed a high longitudinal strength ($Y_1 \equiv \sigma_l$) and a high shear strength ($Y_6 \equiv \tau_c$) such that $Y_1 = Y_6 = \bar{\rho}\sigma_Y$; strain hardening in these directions is neglected. These properties are appropriate for prismatic cores such as the I-core or corrugated core as studied by Côté et al. (2006). The transverse strength Y_2 is assumed to be independent of the plastic strain ε_2^p up to a nominal

densification strain ε_D: beyond densification a linear hardening behaviour is assumed with a very large tangent modulus $E_t = 0.1E_f$. The nominal densification strain is fixed at $\varepsilon_D = 0.85$ while the transverse strength $Y_2 \equiv \sigma_t$ is varied in the parametric studies reported below. The core has a Young's modulus $E_c = \bar{\rho}E_f$ and Poisson's ratio $\nu_c = 0.25$; preliminary numerical simulations confirmed that the predictions are insensitive to the precise magnitude of E_c. The viscosity η of the core is chosen for numerical convenience such that the shock width $l \equiv \eta\varepsilon_D/(\rho_c v_o)$ equals $c/10$ (see for example, Radford et al., 2005). To achieve this shock width, η is adjusted to scale linearly with the estimated peak front face-sheet velocity $v_o = I_T/(\rho_f h)$. This prescription ensures that the shock width is always much less than the core depth yet is adequately resolved by the mesh.[2]

The fluid medium is taken to be water, and is treated here as an acoustic medium of density $\rho_w = 1.0\,\mathrm{Mg\,m^{-3}}$, bulk modulus $K_w = 1.96$ GPa and wave speed $c_w \equiv \sqrt{K_w/\rho_w} = 1400\,\mathrm{ms^{-1}}$. It is assumed that he fluid is unable to sustain tensile loading, and so the cavitation pressure is $p_c = 0$ MPa. A fluid column is used to represent a semi-infinite fluid subjected to a far field explosion. Symmetry boundary conditions are applied to both sides of the fluid column. Acoustic elements are used: four-noded plane strain quadrilateral acoustic elements (R2D2 in ABAQUS notation). A fine mesh is required to ensure minimal numerical dispersion of the blast wave.

3.2. Applied loading

As discussed by McShane et al. (2006), it is desirable to have a small fluid-column with the pressure history, Eq. (1), applied as close to the structure as possible. We thus employ a fluid-column of height $H = 1$ m in all calculations and use the following prescription to ensure minimal reflections from the top of the column, thereby simulating a semi-infinite column. The fluid column is divided into two equal halves, each of height 0.5 m with a horizontal layer of nodes along the interface, hereafter referred to as the 'pressure plane'. The bottom half in contact with the structure is discretised by elements of height 10 mm and the pressure boundary condition (1) is applied to the pressure plane separating the two halves of the fluid column. The top half of the column is discretised using elements of height 40 mm and an *impendence boundary condition* $\dot{u} = p/(\rho_w c_w)$ prescribed on the top surface of the column, where $\dot{u}$ is the particle velocity normal to the top surface and p is the fluid pressure. This boundary condition ensures no reflection of the waves from the top surface thereby simulating a semi-infinite column. The pressure boundary condition (1) is applied in two steps to the nodes of the pressure plane. In step 1, the pressure history (1) is applied for 0.69 ms. The duration of this step is less than the time required for waves reflected from the structure to reach the pressure plane. In step 2, no pressure is specified on the pressure plane. This permits the reflected wave to pass through unimpeded. Although we only specify the pressure history (1) for 0.69 ms, 99.9% of the blast impulse is applied during this period due to the choice $\theta = 0.1$ ms in all calculations.

All calculations were performed for water blasts represented by the free-field pressure versus time characteristic, Eq. (1), with $\theta = 0.1$ ms and p_0 in the range 10–75 MPa. Half of the beam was analysed with symmetry boundary conditions imposed at mid-span, as shown in Fig. 1b. The back (dry) face was fully clamped at the supports, while motion of the core and front face was constrained along the x_1 direction at the supports – this boundary condition is expected to model the loading of a large periodic ship hull structure by a planar blast wave; see Liang et al. (2007) for a discussion of a range of boundary conditions appropriate for modelling such problems. Symmetry boundary conditions were applied to both sides of the fluid column and the loading was prescribed via the water blast pressure history (1). Calculations were also performed on end-clamped monolithic beams. Again, half the beam was analysed with symmetry boundary conditions imposed at mid-span.

3.3. Non-dimensional groups

Following the notation in Tilbrook et al. (2006), we introduce the relevant non-dimensional groups and present all results in Section 4 in terms of these groups. Note that this non-dimensionalisation is only used to present results; the actual numerical calculations were performed using the reference values detailed above.

First, consider the independent groups. The geometry of the beam is specified by

$$\bar{c} \equiv \frac{c}{L} \quad \text{and} \quad \bar{h} \equiv \frac{h}{c}, \tag{10}$$

and the non-dimensional core properties are

$$\bar{\rho} \equiv \frac{\rho_c}{\rho_f}, \quad \bar{\sigma}_l \equiv \frac{\sigma_l}{\bar{\rho}\sigma_Y}, \quad \bar{\sigma}_t \equiv \frac{\sigma_t}{\bar{\rho}\sigma_Y} \quad \text{and} \quad \varepsilon_D. \tag{11}$$

We have normalized the core strengths by $\bar{\rho}\sigma_Y$ so that a core made from the same material as the face-sheets has a non-dimensional strength $0 \leqslant (\bar{\sigma}_l, \bar{\sigma}_t) \leqslant 1$. Note that $\bar{\sigma}_l = 1$ and $\bar{\sigma}_t = 1$ corresponds to a core that achieves the Voigt upper bound on strength in both the transverse and longitudinal directions and this type of core was referred to as the ideal core by Fleck and Deshpande (2004). Additional material non-dimensional groups involving the elastic properties are ε_Y and σ_t/E_c. However, these groups are held constant and in any case do not appreciably affect the results for yield strain values representative of structural alloys. Following Xue and Hutchinson (2004), the non-dimensional water blast impulse is defined by

$$\bar{I}_0 \equiv \frac{2p_0\theta}{M}\sqrt{\frac{\rho_f}{\sigma_Y}}, \tag{12}$$

where $M \equiv (2\bar{h} + \bar{\rho})\bar{c}\rho_f L$ is the mass per unit area of the sandwich beam while the fluid–structure interaction is characterised by the Taylor parameter

$$\psi \equiv \frac{\rho_w c_w \theta}{\rho_f h}. \tag{13}$$

Now, consider the dependent non-dimensional groups. Time t is measured from the instant that the blast wave impinges on the structure. Time is non-dimensionalised by the response time $T \equiv L\sqrt{\rho_f/\sigma_Y}$ of a plastic string of length $2L$ made from a material of yield strength σ_Y and density ρ_f. The transmitted momentum is

$$\bar{I}(\bar{t}) \equiv \frac{I(\bar{t})}{I_0} = \frac{1}{I_0 L}\int_0^L p(x_1, t)\,dx_1 \tag{14}$$

where $p(x_1, \bar{t})$ is the pressure exerted by the fluid on the wet face of the beams at the non-dimensional time $\bar{t} \equiv t/T$. The non-dimensional mid-span front and back face velocities are defined by

$$\bar{v}_f(\bar{t}) \equiv \frac{v_f \rho_f h_f}{I_0} \quad \text{and} \quad \bar{v}_b(\bar{t}) \equiv \frac{v_b \rho_f h_f}{I_0}, \tag{15}$$

respectively, while the normalised final back face deflection at mid-span is defined in terms of the final deflection W_b as $\overline{W}_b \equiv W_b/L$. Finally, we non-dimensionalise the reaction force R at the supports as

[2] Large gradients in stress and strain occur over the shock width and thus a mesh size smaller than l is required to resolve these gradients accurately.

$$\overline{R}(\bar{t}) = \frac{RT}{I_0 L}, \tag{16}$$

so that $\overline{R} = 1$ corresponds to a temporally uniform reaction force capable of arresting a sandwich beam with momentum I_0 in time T.

4. Underwater blast response of sandwich beams

The main aim of this numerical investigation is to study the effect of the beam aspect ratio and transverse core strength on the underwater blast responses of the sandwich beams over a range of blast pressures. All calculations are presented for sandwich beams with aspect ratios ranging from $\bar{c} = 0.1$ to $\bar{c} = 0.3$, face-sheet thickness $\bar{h} = 0.1$ and loaded with water blasts of magnitude $\bar{I}_0 = 0.05$–0.6 and $\psi \equiv \rho_w c_w \theta/(\rho_f h) = 1.875$. Parametric studies are presented where the transverse core strength is varied over the range $0.001 \leqslant \bar{\sigma}_t \leqslant 0.5$.

4.1. Identification of the four regimes

The following four regimes of behaviour of the sandwich beams emerge from the FE calculations presented subsequently:

Regime A: *partial* core densification is completed at the supports *before* the mid-span of the back face begins to decelerate.

Regime B: *full* core densification occurs at the supports *before* the mid-span of the back face begins to decelerate.

Regime C: *partial* core densification is completed of the core at the supports *after* the mid-span of the back face begins to decelerate.

Regime D: *full* core densification occurs at the supports *after* the mid-span of the back face begins to decelerate.

FE simulations to investigate these regimes employed a sandwich beam of geometry $\bar{c} = 0.3$ and $\bar{h} = 0.1$, and subjected to a water blast impulse. The predictions of the mid-span front and rear face velocity versus time histories for transverse core strengths $\bar{\sigma}_t = 0.5$ and 0.001 are shown in Fig. 3. Likewise, predictions for $\bar{\sigma}_t = 0.15$ and 0.007 are given in Fig. 4. These four choices of core strength span the four regimes of behaviour of the sandwich beams. In all cases, the front and back face are stationary until the blast wave impinges upon the front face-sheet. This wave accelerates the front face-sheet over a very short time-scale during which the rear face-sheet remains almost stationary. Subsequently, compression of the core decelerates the front face-sheet and accelerates the

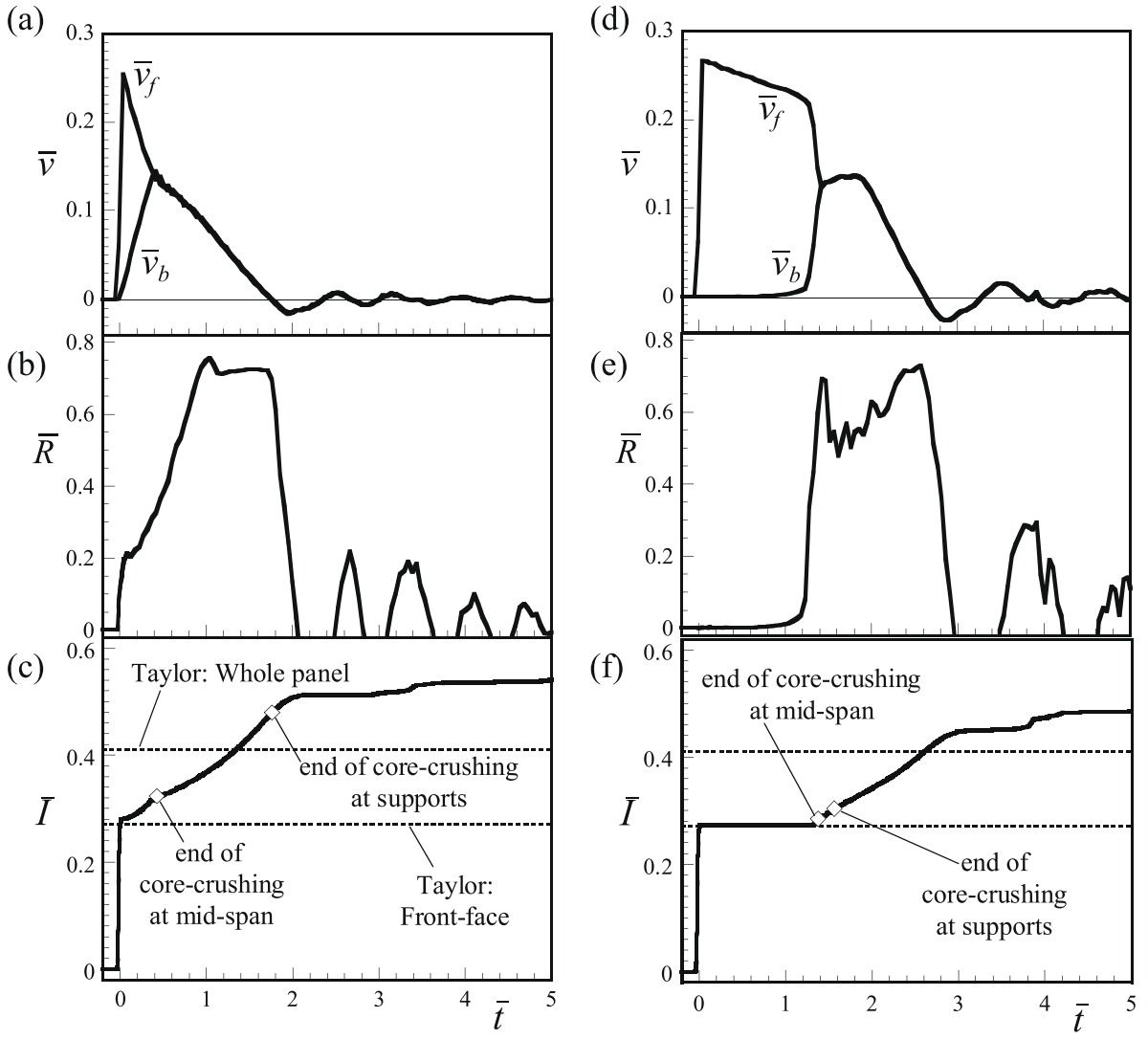

Fig. 3. FE predictions of the temporal variations of the normalised front and back face velocities $\bar{v}_f$ and $\bar{v}_b$, respectively, support reactions $\overline{R}$ and transmitted impulse $\overline{I}$ for sandwich beams with $\bar{c} = 0.3$ subject to an underwater blast impulse $\bar{I}_0 = 0.36$. Plots (a)–(c) are for $\bar{\sigma}_t = 0.5$ while plots (d) through (f) correspond to $\bar{\sigma}_t = 0.001$. All other properties are fixed at their reference values.

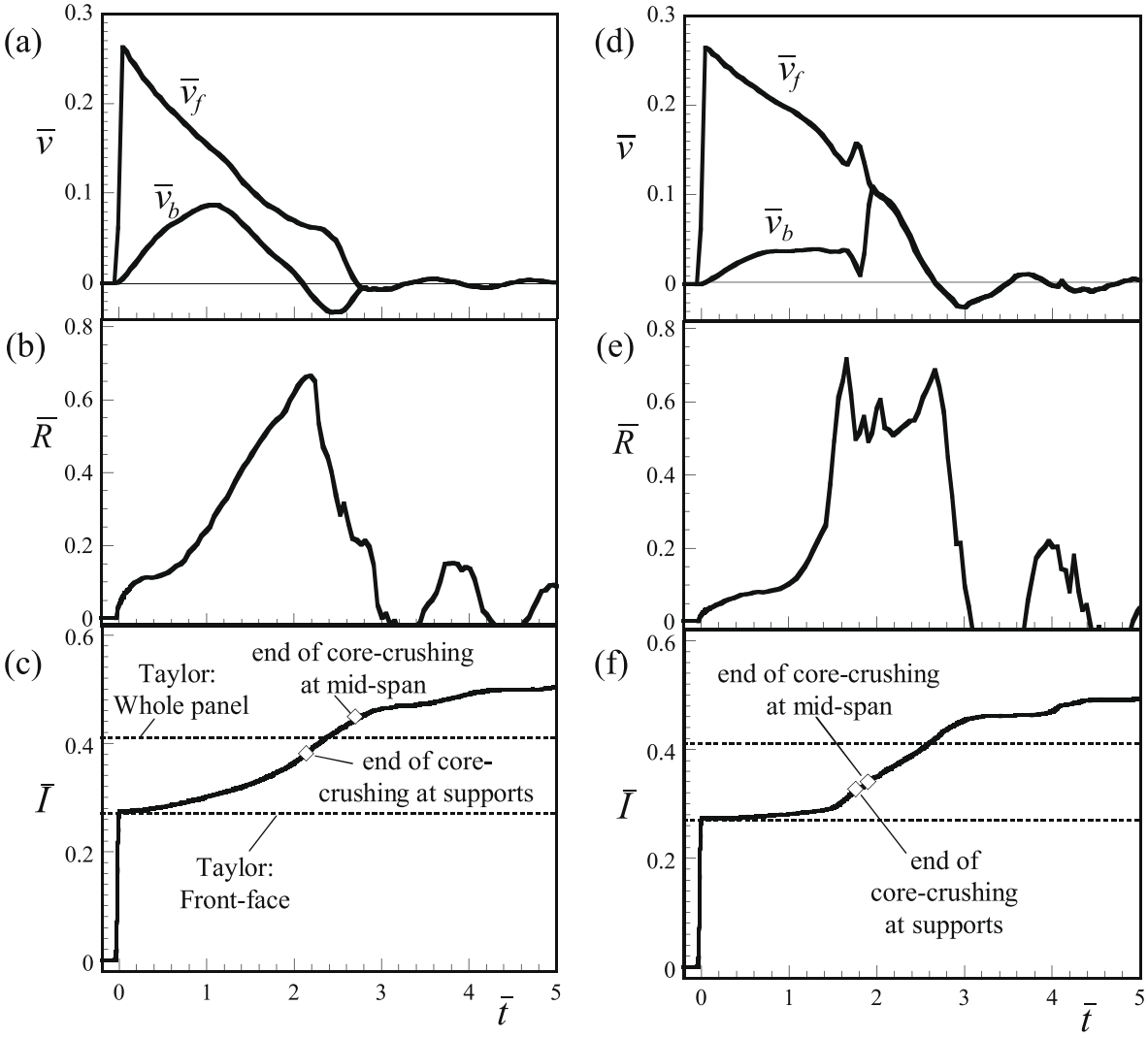

Fig. 4. FE predictions of the temporal variations of the normalised front and back face velocities $\bar{v}_f$ and $\bar{v}_b$, respectively, support reactions $\bar{R}$ and transmitted impulse $\bar{I}$ for sandwich beams with $\bar{c} = 0.3$ subject to an underwater blast impulse $\bar{I}_0 = 0.36$. Plots (a)–(c) are for $\bar{\sigma}_t = 0.15$ while plots (d)–(f) correspond to $\bar{\sigma}_t = 0.07$. All other properties are fixed at their reference values.

back face-sheet. The responses are qualitatively similar to the behaviours shown in Fig. 2 from the impulsive analysis of Tilbrook et al. (2006). We proceed to describe the responses of the sandwich beams after the front face-sheet has attained its peak velocity.

4.1.1. Regime A: decoupled regime with partial core densification ($\bar{\sigma}_t = 0.5$)

The front face velocity decreases linearly with time while the back face velocity increases linearly with time until the face-sheet velocities equalize at mid-span (Fig. 3a). Subsequently, both face-sheets share a common velocity and are brought to rest due to the support reaction. The corresponding normalised support reaction is plotted in Fig. 3b; the support reaction increases up to the instant that the face-sheet velocities equalize at mid-span. Subsequently, the reaction forces remain constant until the sandwich beam has arrested. The accumulated transmitted momentum is shown in Fig. 3c. Three distinct phases of momentum transfer are observed, as follows.

(i) an initial rapid rise during the period when the front face-sheet acquires its maximum velocity. This initial momentum agrees well with the Taylor estimate (Eq. (4)) based upon the front face-sheet mass alone (phase I);

(ii) a more gradual increase in the transmitted momentum during the periods of core compression and beam bending/stretching; and

(iii) a negligible increase in transmitted momentum once the sandwich beam has arrested. It is clear from Fig. 3c that the rate of momentum transfer remains constant after core compression at mid-span has arrested and the beam bending and stretching phases have commenced. This suggests that fluid–structure interaction effects remain significant throughout the response of this sandwich beam. A fully decoupled analysis as suggested by Fleck and Deshpande (2004) may not suffice.

4.1.2. Regime B: decoupled regime with full core densification ($\bar{\sigma}_t = 0.001$)

The choice of a very weak core leads to a negligible deceleration of the front face-sheet and to a negligible acceleration of the front face-sheet. The velocities of the face-sheets equalize rather suddenly upon complete densification of the core at both the supports and mid-span. Subsequently, the mid-span velocities of the face-sheets remain approximately constant while plastic hinges initiate at the supports and travel inwards to mid-span (Fig. 3d). After

these hinges have coalesced at mid-span, the beam arrests by a combination of plastic bending and stretching. The reaction forces at the supports remain small prior to the densification of the cores due to the low core strength: upon core densification the support reactions rise rapidly and remain approximately constant until the beam has arrested (Fig. 3e). The transmitted momentum (Fig. 3f) rises rapidly to the value predicted by Eq. (4) and remains constant at that value until the core has densified fully. Subsequently, the transmitted momentum increases gradually until the beam arrests.

4.1.3. Regime C: coupled regime with partial core densification ($\bar{\sigma}_t = 0.15$)

The temporal variations of the front and back face-sheet velocities plotted in Fig. 4a clearly show that the back face-sheet begins to decelerate before the velocities of the two face-sheet have equalized. In fact, in this case, the back face-sheet arrests before the front face-sheet. The support reactions increase gradually over nearly the entire deformation history of the beam and begin to decrease once the back face-sheet has arrested. The transmitted momentum rises rapidly to the value predicted by (4) during an initial fluid–structure interaction phase and then rises more gradually until the sandwich beam has arrested (Fig. 4c).

4.1.4. Regime D: coupled regime with full core densification ($\bar{\sigma}_t = 0.07$)

Similar to regime C, the front face velocity decreases linearly with time while the back face velocity varies approximately sinusoidally (Fig. 4d). Shortly after the back face has begun to decelerate, full densification of the core occurs both at the supports and at mid-span. Subsequently, the two face-sheets share a common velocity and the sandwich beam is arrested by a combination of bending and stretching. The support reaction rises gradually while the core is compressing and then increases sharply when the core fully densifies. The temporal variation of the transmitted impulse is similar to that of regime C.

It is emphasised that the front face-sheet always acquires its maximum velocity on a time-scale much shorter than the other time-scales involved, viz. the core compression time and the time when the back face begins to decelerate. Thus, based on comparisons of structural time-scales, the regimes of behaviour of sandwich beams subject to water blast are qualitatively similar to impulsively loaded sandwich beams: the fluid structure interaction time-scale t_{cav} does not couple with the other time-scales (t_{eq} and t_{bd}).

4.2. Regime maps

We proceed to present maps of the regimes of behaviour in terms of the above non-dimensional groups. The main aim here is to examine the sensitivity of water blast response to the transverse core strength $\bar{\sigma}_t$ and to the blast impulse $\bar{I}_0$. Maps are plotted with these variables as axes, for the following reference values of properties. The sandwich beams have a face-sheet to core thickness ratio $\bar{h} = 0.1$ and aspect ratio $\bar{c} = 0.3$. A core of relative density $\bar{\rho} = 0.02$ is assumed to have a nominal densification strain $\varepsilon_D = 0.85$ and, consistent with most prismatic core topologies such as the corrugated or diamond core (Côté et al., 2006), the longitudinal and shear strengths are assumed to equal the ideal value of $\bar{\sigma}_l = \bar{\tau}_c = 1$.

The FE predictions of the four regimes of behaviour are illustrated in Fig. 5 on a map with axes $\bar{\sigma}_t$ and $\bar{I}_0$. Regime B (involving full core densification) dominates the map and expands with increasing $\bar{I}_0$ at the expense of all other regimes. Note that the coupled regime with partial core densification (regime C) occurs only over a limited range of $\bar{\sigma}_t$ and the values of $\bar{\sigma}_t$ for regime C increase with increasing $\bar{I}_0$. Contours of normalized final mid-span deflection of the back face-sheet and the maximum reaction forces at the supports are included in Fig. 5a and b, respectively. These contours indicate that both the deflections and support reactions are a minimum in the vicinity of regime C; a discussion on the optimum performance of the beams follows subsequently in Section 4.4.

4.3. Comparison with monolithic beams

It is of practical interest to determine whether sandwich beams are more blast resistant than monolithic beams of equal mass. Appropriate performance metrics are the maximum back face deflection and the maximum support reaction for a given water blast impulse. We now compare the blast resistance for monolithic and sandwich beams of equal mass in order to determine the conditions under which sandwich beams outperform monolithic beams.

The fully-clamped monolithic beams of span $2L$ and thickness H_m are assumed to be made from the same material as the face-sheets of the sandwich beams. In order for the monolithic beams to have the same areal mass M as that of the sandwich beams, the aspect ratio of the monolithic beams is chosen as

$$\frac{H_m}{L} = (2\bar{h} + \bar{\rho})\bar{c}. \tag{17}$$

We write the final mid-span deflection of the back face of the monolithic beam as W_b^{mon} and the maximum support reaction as $R_{\max}^{mon}$. The performance of the sandwich beam relative to the monolithic beam is quantified by the ratios W_b/W_b^{mon} and R_{max}/R_{max}^{mon}, where W_b and R_{max} denote the final back face deflection and maximum support reaction, respectively, of the sandwich beam. These are plotted as a function of the transverse core strength $\bar{\sigma}_t$ in Fig. 6 for $\bar{c} = 0.3$ and for selected values of $\bar{I}_0$. The active regimes, as ascertained by the criteria of Section 4.1, are indicated in Fig. 6. The transition with increasing core strength from regimes B → D → C → A is generally observed. For nearly all values of $\bar{\sigma}_t$, the sandwich beams deflect less than monolithic beams of equal mass (Fig. 6a) and can be as low as 20% of that of their monolithic counterparts for low values of $\bar{I}_0$. A clear optimum value of $\bar{\sigma}_t$ that minimizes $\overline{W}_b$ for a given $\bar{I}_0$ is observed. Note that this optimum core strength increases with increasing $\bar{I}_0$. Similarly, the support reactions of the sandwich beams are smaller than those for the monolithic beams of equal mass (Fig. 6b) over the entire range of $\bar{I}_0$ and $\bar{\sigma}_t$ investigated here. However, from a comparison of Fig. 6a and b we deduce that the value of $\bar{\sigma}_t$ that minimizes the deflection of the sandwich beam at a given value of $\bar{I}_0$ does not minimize the reaction force.

4.4. Optimal performance of the sandwich beams

The results presented above indicate that there exists a narrow range of transverse core strength values over which the sandwich beams exhibit an optimal performance in terms of minimizing the back face deflection or support reaction. We envisage a design situation for blast resistant sandwich beams where, for a given sandwich beam aspect ratio $\bar{c}$, the aim is to determine the optimal value of $\bar{\sigma}_t$ as a function of the water blast impulse $\bar{I}_0$. Performance is assessed in terms of (a) final back-face deflection and (b) peak reaction load at the supports and the optimal core strength is defined as that which minimizes either the back face deflections or support reactions.

Fig. 5a shows a design chart with axes $\bar{I}_0$ and $\bar{\sigma}_t$ for sandwich beams with aspect ratio $\bar{c} = 0.3$. Contours of the FE predictions of the non-dimensional maximum mid-span back face deflection $\overline{W}_b$ are included in Fig. 5a for the purposes of selecting the core strengths that minimize the back face deflections for a given value of $\bar{I}_0$. The trajectory of arrows in Fig. 5a traces the optimum designs

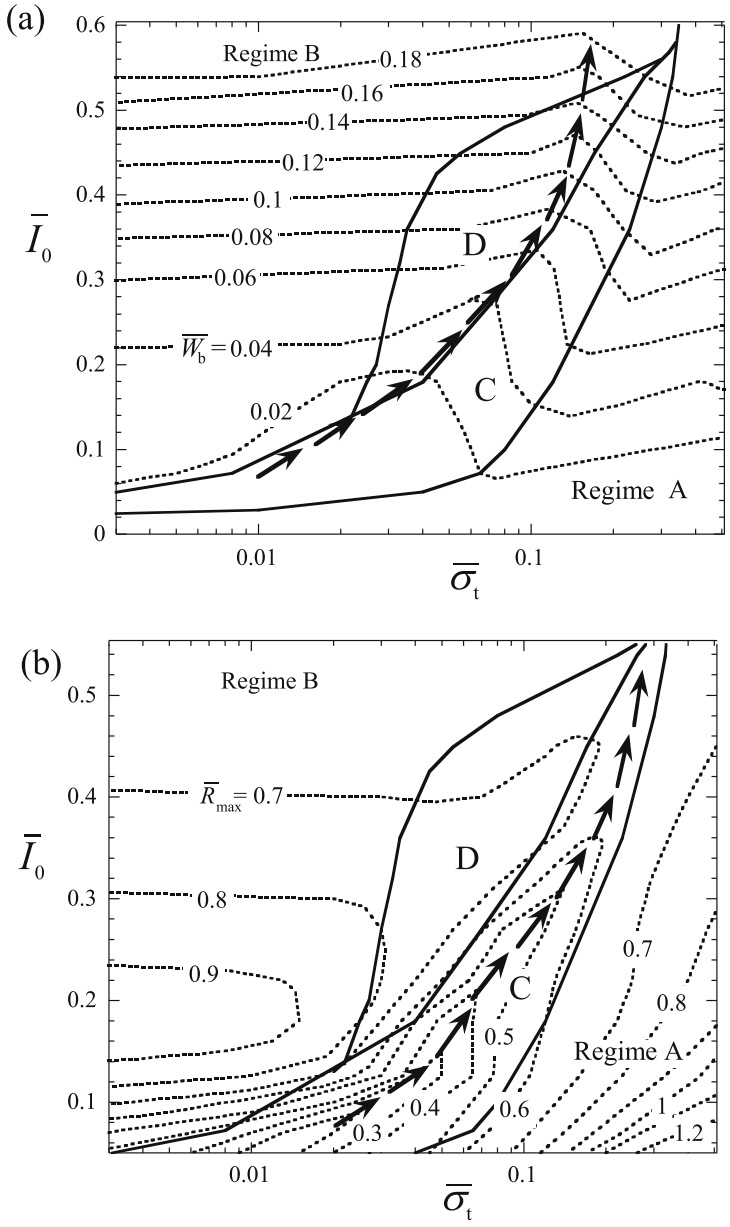

Fig. 5. Design charts for $\bar{c} = 0.3$ sandwich beams with axes $\bar{I}_0$ and $\bar{\sigma}_t$. (a) FE predictions of the contours of the normalised permanent mid-span back face deflections $\overline{W}_b$. The thick solid lines denote the FE predictions of the regime boundaries. (b) FE predictions of contours of normalised peak support reaction force $\overline{R}_{max}$. The regime boundaries from fully-coupled fluid–structure FE simulations are included. All other properties are fixed at their reference values.

with increasing $\bar{I}_0$ (i.e. the core strength $\bar{\sigma}_t$ that minimize $\overline{W}_b$ for a series of fixed values of $\bar{I}_0$). The optimum designs lie near the boundary between regimes C and D for lower applied impulses and lie on a trajectory through regime D into B for higher applied impulses. Note that the optimum value of the core strength $\bar{\sigma}_t^{opt}$ increases with increasing $\bar{I}_0$ – for a representative blast impulse of $\bar{I}_0 \approx 0.4$, $\bar{\sigma}_t^{opt} \approx 0.1$ which corresponds to a core of compressive strength 0.4 MPa in the case of a sandwich beam made from alloy with a yield strength $\sigma_Y = 200$ MPa and a core of relative density $\bar{\rho} = 0.02$.

Alternatively, to minimize the support reactions, we plot in Fig. 5b the FE predictions of the normalised maximum support reaction $\overline{R}_{max}$. The trajectory of arrows traces the path of optimum designs (i.e. core strengths $\bar{\sigma}_t^{opt}$ that minimize $\overline{R}_{max}$ for a given $\bar{I}_0$) with increasing $\bar{I}_0$. This path approximately follows the centre of regime C. Note that these optimum designs do not lie in the regimes of full densification; there is a sharp rise in the support reaction near the boundary between partial densification and full densification. The predictions of the optimum strengths $\bar{\sigma}_t^{opt}$ (to minimize either $\overline{W}_b$ or $\overline{R}_{max}$) for the $\bar{c} = 0.3$ sandwich beam are plotted in Fig. 9 as a function of the water blast impulse $\bar{I}_0$. Over the entire range of $\bar{I}_0$ considered, the $\bar{\sigma}_t^{opt}$ values required to minimize $\overline{R}_{max}$ are about 40% higher than those required to minimize $\overline{W}_b$. Predictions for optimal core strength (to minimize $\overline{W}_b$) from the impulsive loading analytical model of Tilbrook et al. (2006) are included in Fig. 9, with the impulse transmitted to the front face-sheet estimated using Eq. (4). It is apparent that these analytical predictions overestimate and underestimate the values of $\bar{\sigma}_t^{opt}$ for low and high values of $\bar{I}_0$, respectively.

5. Discussion: decoupled versus coupled fluid structure interaction simulations

The significance of continued fluid loading during all stages of sandwich beam response is now assessed by performing a series

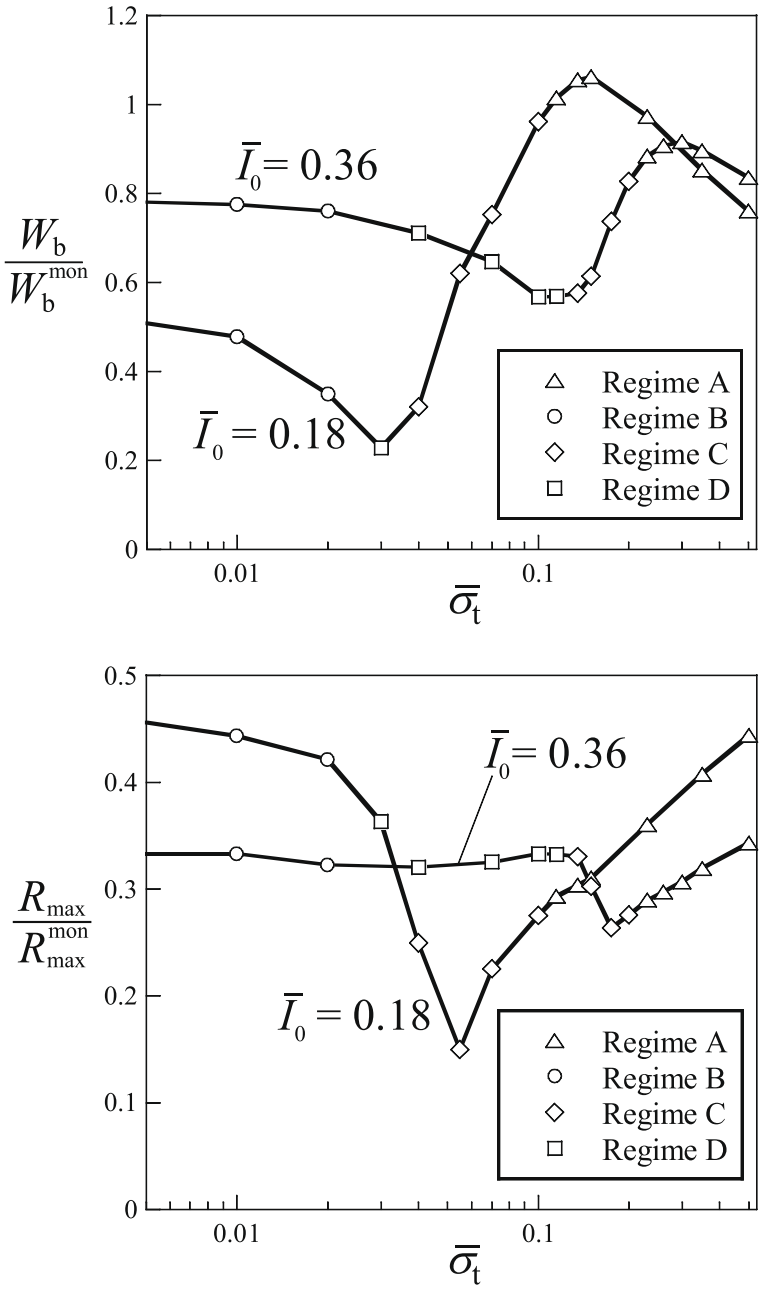

Fig. 6. Finite element predictions of sandwich beams ($\bar{c} = 0.3$) and monolithic beams of equal mass. (a) The permanent mid-span back face deflections W_b and (b) peak support reactions forces R_{max} of sandwich beams normalised by the corresponding values W_b^{mon} and R_{max}^{mon} of monolithic beams for two selected values of $\bar{I}_0$. Predictions are shown for a range of transverse core strengths $\bar{\sigma}_t$. All other properties of the sandwich beam are fixed at the reference values.

of additional FE calculations on a clamped sandwich beam with the fluid absent. These *decoupled* calculations assume an initial momentum I_T in the front (dry) face of the sandwich beam. This momentum is specified either by (5) or by the final acquired momentum in a separate FE simulation of a free-standing sandwich beam subjected to the same water blast loading. Note that the free-standing beam calculation is one-dimensional.

We begin by comparing the momentum versus time histories for a fully clamped beam and for a free-standing beam. The temporal variation of the momentum transmitted into the clamped and free-standing beams is plotted in Fig. 7a and b for blast impulses $\bar{I}_0 = 0.18$ and 0.36, respectively. The sandwich beams in these calculations have reference properties with $\bar{\sigma}_t = 0.1$. For both the clamped and free-standing beams, there is a rapid initial rise in the transmitted momentum with a knee in the $\bar{I}(\bar{t})$ curve at approximately the Taylor value, Eq. (4), of the transmitted momentum considering the front face mass only. Subsequently, the free standing beams acquire a small additional momentum until the end of core compression. For both values of $\bar{I}_0$ considered, the total momentum transferred into the clamped beams is greater than the free-standing beams. However, in addition to the momentum transfer, the rate of momentum transfer (or equivalently the pressure exerted by the fluid on the sandwich beam) is a critical factor in governing the deformation of the beams. We observe that the rate of momentum transfer is also greater for the clamped beam than for the free-standing beam. In fact, for $\bar{I}_0 = 0.36$, the pressure exerted by the fluid on the sandwich beams increases after the end of core compression. Fluid–structure interaction effects remain sig-

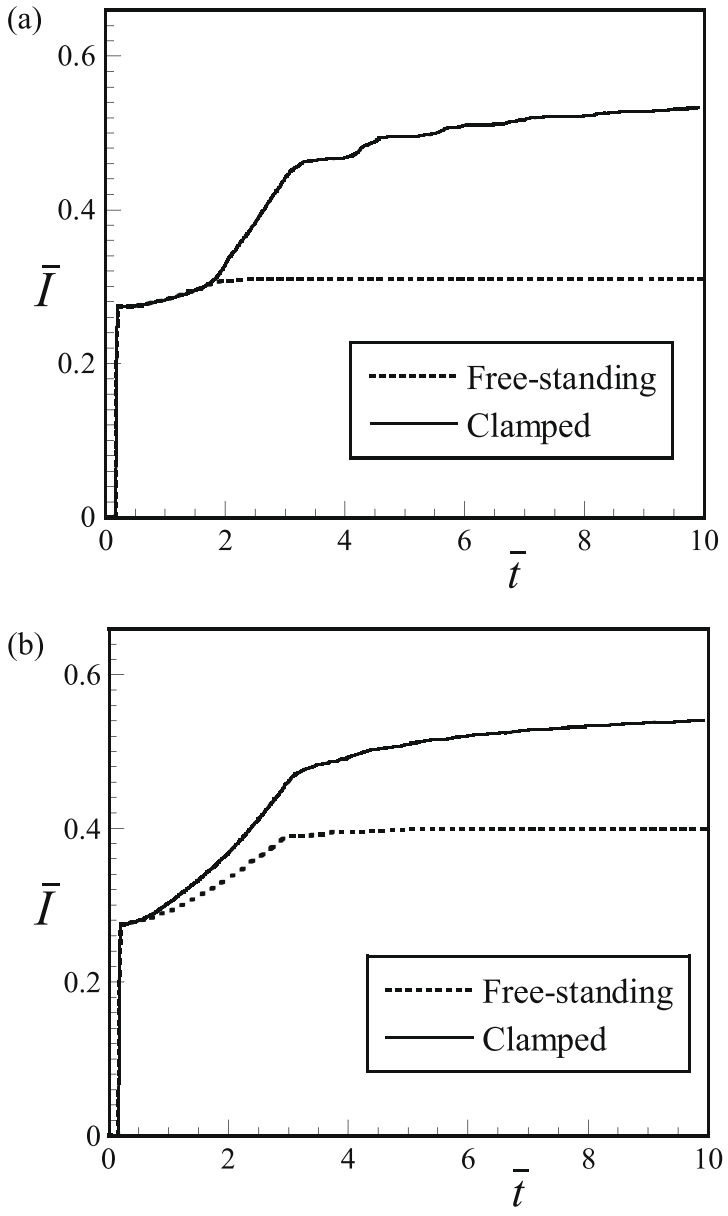

Fig. 7. Comparison of the transmitted impulse $\bar{I}$ for free-standing and clamped sandwich beams. FE results are shown for sandwich beams with $\bar{\sigma}_t = 0.1$ and $\bar{c} = 0.3$ subject to blast impulses (a) $\bar{I}_0 = 0.36$ and (b) $\bar{I}_0 = 0.18$. All other properties are fixed at their reference values.

nificant during the beam bending and stretching phases of the motion.

It is instructive to compare the mid-span beam deflections for the fluid-loaded, end-clamped beam with that for an impulsively loaded end-clamped beam absent the fluid. Recall that the initial impulse I_T is provided to the front (dry) face and is either estimated by (5) or is equated to the final momentum in a one-dimensional, fluid-loaded free-standing beam. In the FE simulation of this free-standing beam, the same water blast parameters are used as for the corresponding end-clamped beam.

Comparisons between the decoupled and fully-coupled fluid–structure interaction predictions of the maximum mid-span deflections of the back face of the sandwich beams are shown in Fig. 8a as a function of $\bar{\sigma}_t$ for the choice $\bar{c} = 0.3$ and selected values of $\bar{I}_0$.

At low values of $\bar{I}_0$, the decoupled calculations are in reasonable agreement with the fully-coupled predictions. At the higher values of $\bar{I}_0$, the decoupled calculations using the transmitted impulse estimated from free-standing beam calculations, and the Taylor estimate based on the entire mass of the sandwich beam, under-predict and over-predict $\overline{W}_b$, respectively. In fact, the predictions in Fig. 8a indicate that these two sets of the decoupled predictions approximately bound the full-coupled predictions of $\overline{W}_b$. Similar conclusions are drawn for the sandwich beams with $\bar{c} = 0.1$ (Fig. 8b).

6. Concluding remarks

The water blast response of sandwich beams has been investigated using finite element simulations. It is demonstrated that appropriately designed sandwich beams significantly outperform monolithic beams of equal mass based on either minimizing back face deflections or support reaction forces.

Over the parameter range investigated here, the front face acquires its maximum velocity on a much smaller time-scale than the core compression and back face response times. Thus, the *ini-*

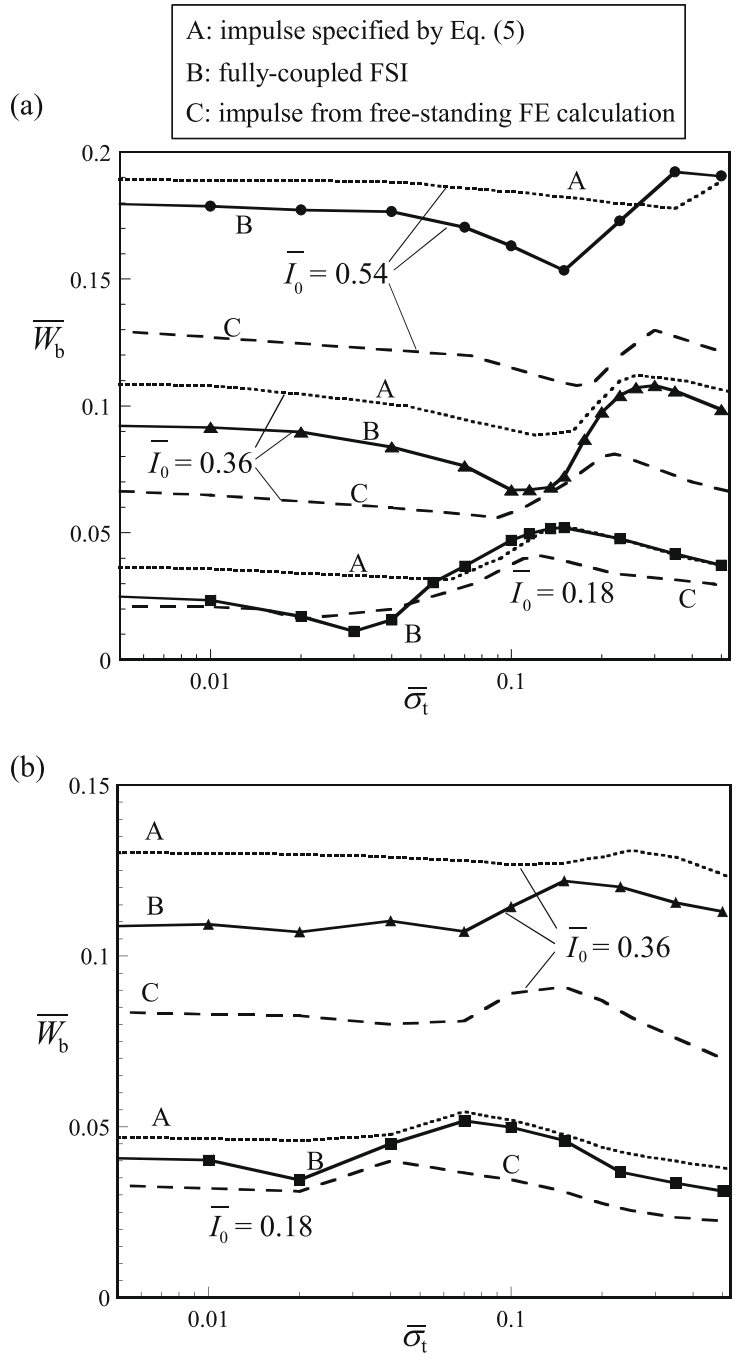

Fig. 8. The normalized deflection $\overline{W}_b$ for A: decoupled simulations with impulse specified by Eq. (5); B: fully coupled simulations and C: decoupled simulations with the impulse obtained from FSI calculations on free-standing panels. Results are shown for (a) $\bar{c} = 0.3$ and (b) $\bar{c} = 0.1$ for selected value of $\bar{I}_0$ as a function of $\bar{\sigma}_t$. All other properties are fixed at their reference values.

tial stage of fluid–structure interaction decouples from the other structural time-scales. Continued fluid loading occurs after initial cavitation, and this couples with the structural response. A fully decoupled analysis, as proposed by Fleck and Deshpande (2004), is most appropriate for sandwich beams with a high transverse core strength, and subjected to relatively low levels of blast impulse.

Four distinct regimes of behaviour emerge from the FE calculations based on the relative time-scale of the back face response and the time required to equalize the front and back face velocities. Maps showing the dominance of the four regimes are constructed to illustrate the effect of the sandwich beam aspect ratio $\bar{c}$, transverse core strength $\bar{\sigma}_t$ and blast impulse $\bar{I}_0$ upon the type of response.

For a given blast impulse and sandwich beam geometry there exists an optimum transverse core strength that minimizes the back face deflection. The optimal core strength to minimize the support reactions is typically 40% above that required to minimize the back face deflection. These optimal values of core strength increase with increasing blast impulse and thus a sandwich beam designed to be optimal for a given blast impulse is suboptimal for other blast loadings.

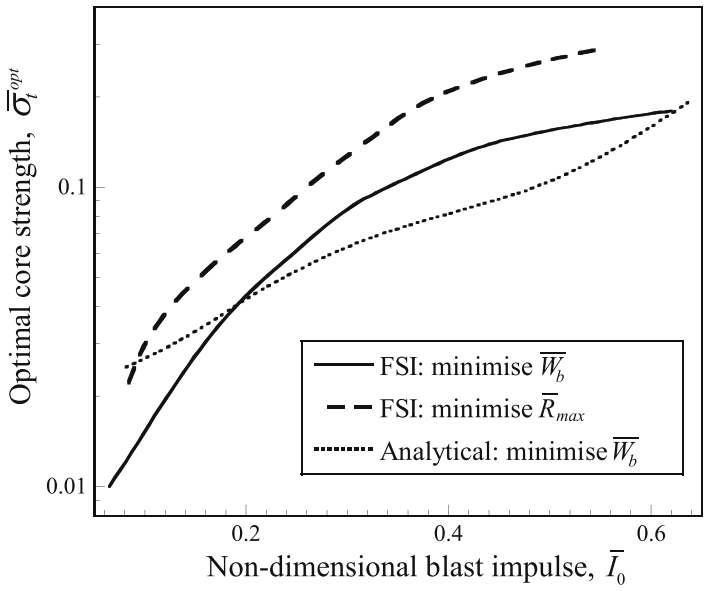

Fig. 9. Predictions of the optimal core strength $\bar{\sigma}_t^{opt}$ for $\bar{c} = 0.3$ sandwich beams as a function of the blast impulse $\bar{I}_0$. All other properties are fixed at their reference values. Fully coupled fluid–structure interaction (FSI) predictions of the optimum strength in order to minimize either $\overline{W}_b$ or $\overline{R}_{\max}$ are shown. In addition predictions obtained using the impulsive loading analytical estimates of Tilbrook et al. (2006) are also included in which the transmitted impulse is estimated from Eq. (4).

Acknowledgment

The authors are grateful to ONR for their financial support through US-ONR IFO Grant No. N00014-03-1-0283 on The Science and Design of Blast Resistant Sandwich Structures.

References

Balden, V.H., Nurick, G.N., 2005. Numerical simulation of the post-failure motion of steel plates subjected to blast loading. International Journal of Impact Engineering 32, 14–34.

Cole, R.H., 1948. Underwater Explosions. Princeton University Press, Princeton, NJ.

Côté, F., Deshpande, V.S., Fleck, N.A., Evans, A.G., 2006. The compressive and shear responses of corrugated and diamond lattice materials. International Journal of Solids and Structures 43, 6202–6242.

Deshpande, V.S., Fleck, N.A., 2005. A. One-dimensional response of sandwich plates to underwater shock loading. Journal of the Mechanics and Physics of Solids 53 (11), 2347–2383.

Fleck, N.A., Deshpande, V.S., 2004. The resistance of clamped sandwich beams to shock loading. Journal of Applied Mechanics 71 (3), 386–401.

Hanssen, A.G., Enstock, L., Langseth, M., 2002. Close-range blast loading of aluminum foam panels. International Journal of Impact Engineering 27, 593–618.

Hutchinson, J.W., Xue, Z., 2005. Metal sandwich plates optimised for pressure pulses. International Journal of Mechanical Sciences 47 (4–5), 545–569.

Jones, N., 1971. A theoretical study of the dynamic plastic behavior of beams and plates with finite deflections. International Journal of Solids and Structures 7, 1007–1018.

Jones, N., 1989. Structural Impact. Cambridge University Press, Cambridge, UK.

Lee, Y.-W., Wierzbicki, T., 2005a. Fracture prediction of thin plates under localized impulsive loading. Part I: dishing. International Journal of Impact Engineering 31, 1253–1276.

Lee, Y.-W., Wierzbicki, T., 2005b. Fracture prediction of thin plates under localized impulsive loading. Part II: discing and petalling. International Journal of Impact Engineering 31, 1277–1308.

Liang, Y., Spuskanyuk, A.V., Flores, S.E., Hayhurst, D.R., Hutchinson, J.W., McMeeking, R.M., Evans, A.G., 2007. The response of metallic sandwich panels of water blast. Journal of Applied Mechanics 74, 81–99.

McShane, G.J., Deshpande, V.S., Fleck, N.A., 2007. The underwater blast resistance of metallic sandwich beams with prismatic lattice cores. Journal of Applied Mechanics 74, 352–364.

Menkes, S.B., Opat, H.J., 1973. Tearing and shear failure in explosively loaded clamped beams. Experimental Mechanics 13, 480–486.

Nesterenko, V.F., 2003. Shock (blast) mitigation by soft condensed matter. MRS Symposium Proceedings 759, 4.3.1–4.3.12.

Nurick, G.N., Shave, G.C., 2000. The deformation and tearing of thin square plates subjected to impulsive loads- an experimental study. International Journal of Mechanical Sciences 18, 99–116.

Paik, J.K., 2003. Innovative structural designs of tankers against ship collisions and grounding: a recent state-of-the-art review. Marine Technology 40, 25–33.

Rabczuk, T., Kim, J.Y., Samaniego, E., Belytschko, T., 2004. Homogenization of sandwich structures. International Journal for Numerical Methods in Engineering 61 (7), 1009–1027.

Radford, D.D., Deshpande, V.S., Fleck, N.A., 2005. The use of metal foam projectiles to simulate shock loading on a structure. International Journal of Impact Engineering 31 (9), 1152–1171.

Swisdak, M.M., 1978. Explosion effects and properties – part II: explosion effects in water, Technical Report, Naval Surface Weapons Center, Dahlgren, VA.

Symmonds, P.S., 1954. Large plastic deformation of beams under blast type loading. Second US National Congress of Applied Mechanics.

Taylor, G.I., 1941. The pressure and impulse of submarine explosion waves on plates. The Scientific Papers of G.I. Taylor, vol. III. Cambridge University Press, 1963, pp. 287–303.

Tilbrook, M.T., Deshpande, V.S., Fleck, N.A., 2006. Regimes of response for impulse-loaded sandwich panels. Journal of the Mechanics and Physics of Solids 54 (11), 2242–2280.

Wang, A.J., Hopkins, H.G., 1954. On the plastic deformation of built-in circular plates under impulsive load. Journal of the Mechanics and Physics of Solids 3, 22–37.

Wei, Z., Deshpande, V.S., Evans, A.G., Dharmasena, K.P., Queheillalt, D.T., Wadley, H.N.G., Murty, Y., Elzey, R.K., Dudt, P., Chen, Y., Knight, D., Kiddy, K., 2007. The resistance of metallic plates to localized impulse. Journal of the Mechanics and Physics of Solids. doi:10.1016/j.jmps.2007.10.010.

Xue, Z., Hutchinson, J.W., 2004. A comparative study of blast-resistant metal sandwich plates. International Journal of Impact Engineering 30 (10), 1283–1305.

Yen, C.F., Skaggs, R., Cheeseman, B.A., 2005. Modeling of shock mitigation by sandwich structures for blast protection. The International Conference on Structural Stability and Dynamics, Kissimmee, FL.